Imaging the geometrical structure of the H_2^+ molecular ion by high-order above-threshold ionization in an intense laser field

Yingchun Guo,[1,2] Panming Fu,[1] Zong-Chao Yan,[3,4] Jiangbin Gong,[5] and Bingbing Wang[1,*]

[1]*Laboratory of Optical Physics, Beijing National Laboratory for Condensed Matter Physics, Institute of Physics, Chinese Academy of Sciences, Beijing 100080, China*

[2]*State Key Laboratory of Precision Spectroscopy, East China Normal University, Shanghai 200062, China*

[3]*Department of Physics, University of New Brunswick, P.O. Box 4400, Fredericton, New Brunswick, Canada E3B 5A3*

[4]*Center for Theoretical Atomic and Molecular Physics, The Academy of Fundamental and Interdisciplinary Sciences, Harbin Institute of Technology, Harbin 150080, China*

[5]*Department of Physics and Center of Computational Science and Engineering, National University of Singapore, Singapore 117542, Singapore*

(Received 27 May 2009; revised manuscript received 8 October 2009; published 4 December 2009)

Using a frequency-domain theory, we demonstrate that an angle-resolved high-order above-threshold ionization (HATI) spectrum carries three pieces of important information: the fingerprint of the molecular wave function in the direct above-threshold-ionization amplitude, the geometrical structure of the molecule in the potential scattering between two plane waves, and the interaction between the ionized electron and the laser field, manifested in a phase factor associated with laser-assisted collisions. As a result all main interference features in the HATI spectrum can be physically explained. As an application it is pointed out that the skeleton structure of a molecule can be better imaged using lasers of higher frequencies.

DOI: 10.1103/PhysRevA.80.063408 PACS number(s): 32.80.Rm, 33.80.−b, 42.50.Hz, 42.65.−k

Laser-driven rescattering processes of electrons have opened up novel means for molecular structure imaging. Of vast interest are high-order harmonic generation (HHG) [1–3] and high-order above-threshold ionization (HATI) [4–8] processes. Odžak and Milosevic [2] showed that clear minima on HHG spectra reveal molecular orientation. Becker *et al.* [7] demonstrated that the interference structure of a HATI spectrum reflects the symmetry of the ground-state molecular orbital. Further, a general cosine formula describing the destructive interference of a multiple-center recollision was found in both HHG [2] and HATI [7] spectra. However, such a simple function does not suffice to extract more structure information from the HATI spectrum. Hence it is important to find the origin of the interference pattern in the HATI spectrum and the relationship between the interference and the characteristics of the molecule-laser system. As an example, we note the recent work of Okunishi *et al.* [8], which showed orientation-averaged angle-resolved HATI spectra. Therein the interference fringes in the HATI spectra predicted by theoretical calculations are apparent but the underlying physics is not understood.

In this paper, via a frequency-domain theory based on the strong-field approximation, we expose three important aspects of a HATI spectrum. In particular, we demonstrate that an angle-resolved HATI spectrum carries three pieces of information: the fingerprint of a molecular wave function, the geometrical structure of a molecule, and the interaction between the ionized electron and the laser field. As such, for the first time, the physical origins of the interference features in the HATI spectrum become all clear. As an application of this study, we demonstrate that the molecular skeleton structure can be better imaged as the laser frequency becomes higher. We note the relevant work by Reiss on the ATI of an atom in a low frequency laser field also using the strong-field approximation [9].

The frequency-domain theory based on a nonperturbative quantum electrodynamics was developed by Guo *et al.* [10] in 1989 dealing with the above threshold ionization (ATI). Gao *et al.* [11] then extended it to HHG process. Fu *et al.* [12] demonstrated the relationship between the time-domain and frequency-domain theories in strong-field physics. Wang *et al.* [13] also used the frequency-domain theory to investigate HATI processes. As seen below, in the frequency-domain or time-independent picture, the dynamics of a rescattering process can be understood as a two-step transition. Therefore, the HATI of a molecule in a strong laser field can be treated as an ATI followed by a laser-assisted collision (LAC).

Consider now a molecule interacting with a quantized single-mode laser field of frequency ω. The Hamiltonian for the molecule-laser system is $H=H_0+U(\mathbf{r})+V$, where $H_0=\frac{(-i\nabla)^2}{2m_e}+\omega N_a$ is the energy operator for a free electron-photon system, N_a is the photon number operator, $U(\mathbf{r})$ is the molecular binding potential, and V is the electron-photon interaction. Atomic units are used throughout unless otherwise stated. The time-independent feature of the field-quantized Hamiltonian enables us to treat HATI as a genuine scattering process in an isolated system that consists of the photons and the molecule, where the formal scattering theory [14] can be applied. Therefore, the transition matrix element can be written as [10,13]

$$T_{fi}=\langle\psi_f|V|\psi_i\rangle+\langle\psi_f|U\frac{1}{E_f-H+i\epsilon}V|\psi_i\rangle, \tag{1}$$

where the initial state $|\psi_i\rangle=|\Phi_i(\mathbf{r}),n_i\rangle=\Phi_i(\mathbf{r})\otimes|n_i\rangle$ is the eigenstate of the Hamiltonian $H_0+U(\mathbf{r})$ with the associated

*Author to whom correspondence should be addressed.

energy $E_i=-E_B+(n_i+\frac{1}{2})\omega$. Moreover, $\Phi_i(\mathbf{r})$ is the ground-state wave function of the molecular electron with the binding energy E_B and $|n_i\rangle$ is the Fock state of the laser mode with the photon number n_i. The final state $|\psi_f\rangle=|\Psi_{\mathbf{p}_f n_f}\rangle$ of energy $E_f=E_{\mathbf{p}_f n_f}$ is the Volkov state of the quantized field [10,13]. In constructing this final state, the molecular binding potential is assumed to be weak as compared to the laser field. Correction to the Volkov state can be made by, for example, applying the Coulomb-Volkov state [15] in the theory. However, such a correction is not essential for our purpose here.

The first and second terms in Eq. (1) correspond to the processes of direct and rescattering ATI, respectively. Thus, T_{fi} can be expressed as $T_{fi}=T_{\mathrm{d}}+T_{\mathrm{r}}$. On the one hand, as for the direct ATI transition, we have [10,16] $T_{\mathrm{d}}=\langle\psi_f|V|\psi_i\rangle=V_e^{-1/2}\omega(u_p-j)\Phi(\mathbf{p}_i)\mathcal{J}_j(\zeta_f,\eta)$, where V_e is the normalization volume of the field, and $u_p=U_p/\omega$ with U_p the ponderomotive energy of an electron in the laser field, $j=n_i-n_f$, $\Phi(\mathbf{p}_i)$ is the Fourier transform of the initial wave function $\Phi_i(\mathbf{r})$, and $\mathcal{J}_j(\zeta_f,\eta)=\Sigma_{m=-\infty}^{\infty}J_{-j-2m}(\zeta_f)J_m(\eta)$ is the generalized Bessel function with $\zeta_f=2\sqrt{u_p/\omega}\mathbf{p}_f\cdot\hat{\boldsymbol{\epsilon}}$, $\mathbf{p}_f$ the momentum of the electron in the finial state, $\hat{\boldsymbol{\epsilon}}$ the polarization vector of the laser field, and $\eta=u_p/2$. Note that since the T_{d} transition contains the molecular wave function, the direct ATI spectrum can be used to image the characteristic of a molecular wave function. As an example, we calculate the angle-resolved direct ATI spectra for O_2 and N_2 molecule with the molecular axis along the laser polarization with $\omega=0.114$ and $U_p=2\omega$. The wave function of O_2 or N_2 is the same as in [17]. The angle θ_f is between the final momentum of the ionized electron and the molecular axis. We find that for N_2 the ATI rate decreases with θ_f. For O_2, the ATI rate is zero at $\theta_f=0$. It then increases rapidly with θ_f reaching its maximum at about 20°, and then decreases. These results agree qualitatively well with the work by Chen *et al.* [17].

On the other hand, the rescattering ATI transition can be written as [13] $T_{\mathrm{r}}=-i\pi\Sigma_{\text{all channels}}T_{\mathrm{LAC}}T_{\mathrm{ATI}}\delta(E_f-E_{\mathbf{p}_1 n_1})$, where $T_{\mathrm{ATI}}=\langle\Psi_{\mathbf{p}_1 n_1}|V|\Phi_i,n_i\rangle$ and $T_{\mathrm{LAC}}=\langle\Psi_{\mathbf{p}_f n_f}|U|\Psi_{\mathbf{p}_1 n_1}\rangle$. The physics underlying T_{r} transition is as follows. Specifically, T_{ATI} represents the direct ATI amplitude, where the ground-state electron absorbs n_i-n_1 photons from the laser field and ionizes; whereas T_{LAC} represents the amplitude of LAC in which the ionized electron absorbs n_1-n_f photons from the field during its collision with the nucleus, resulting in the change of the canonical momentum of the electron from $\mathbf{p}_1$ to $\mathbf{p}_f$. Therefore, from the frequency-domain picture, the rescattering ATI can be described simply as an ATI followed by a LAC with all ATI channels summed up coherently. Furthermore, the T_{r} transition indicates that T_{ATI} provides a weighting amplitude for T_{LAC} transition in each ATI channel. The interesting fact is that because the initial molecular wave function only appears in the T_{ATI} term, it can only influence the amplitude of LAC transition for each ATI channel, resulting in that the wave function can only affect the HATI amplitude, rather than the interference pattern of the HATI spectrum. This finding can explain the difference of the angle-resolved HATI spectra for O_2 and N_2 by Becker *et al.* in [7].

The ATI transition T_{ATI} in T_{r} has the same form as T_{d} transition with $\mathbf{p}_f$ and n_f being replaced by $\mathbf{p}_1$ and n_1, respectively. On the other hand, the transition matrix element of LAC can be written as

$$T_{\mathrm{LAC}}=V_e^{-1}J_s(\zeta_1-\zeta_f)\langle\mathbf{p}_f|U|\mathbf{p}_1\rangle=V_e^{-1}\frac{\omega}{2\pi}\langle\mathbf{p}_f|U|\mathbf{p}_1\rangle\Delta\Theta, \tag{2}$$

where J_s is the Bessel function with $s=n_1-n_f$ and $\zeta_1=2\sqrt{u_p/\omega}\mathbf{p}_1\cdot\hat{\boldsymbol{\epsilon}}$, and $\Delta\Theta=\int_0^T dt\,\exp\{-i[s\omega t+(\zeta_1-\zeta_f)\sin\omega t]\}$. To obtain the last equation, we use the integral representation of the Bessel function. Equation (2) indicates that the LAC can be understood as the potential scattering between two plane waves, as shown by $\langle\mathbf{p}_f|U|\mathbf{p}_1\rangle=\int d\mathbf{r}\,\exp[-i(\mathbf{p}_f-\mathbf{p}_1)\cdot\mathbf{r}]U(\mathbf{r})$, with a phase factor $\Delta\Theta$ reflecting the sum of the phase difference between the two states before and after the collision within one optical cycle $T=2\pi/\omega$. The existence of the phase factor is due to the fact that the recolliding electron oscillates by the laser field during the recollision process. Thus, the interference pattern of the molecular HATI spectrum can be attributed to the combination of the potential scattering and the phase factor $\Delta\Theta$. In particular, the skeleton structure of the molecule lies in the potential scattering term, while the interaction between the ionized electron and the laser field is represented by the phase factor term in Eq. (2). Since the phase factor is independent of the potential scattering term and is only determined by the laser condition, it provides a "background" of interference fringes. This being the case, the phase factor $\Delta\Theta$ is a common factor for both the molecular and atomic systems.

We now focus on the imaging of the geometrical structure of a molecule, rather than its wave function, by HATI spectrum. We consider a HATI process of H_2^+ in an intense laser field. For illustration purpose a zero-range potential model is employed for $U(\mathbf{r})$, as in [4]. That is, $U_0(\mathbf{r})=\frac{2\pi}{\kappa}\delta(\mathbf{r})\frac{\partial}{\partial r}r$, with $\kappa=\sqrt{2|E_B|}$, and the two-center binding potential of a diatomic molecule becomes $U(\mathbf{r})=U_0(\mathbf{r}-\mathbf{z}_0)+U_0(\mathbf{r}+\mathbf{z}_0)$, where $-\mathbf{z}_0$ and $+\mathbf{z}_0$ are the positions of the two nuclei. The molecular orientation is along the polarization of the laser field and the internuclear separation R_0 is 2 a.u. The wave function of H_2^+ is $\Phi_i(\mathbf{r})=\frac{1}{\sqrt{2(1+C)}}[\phi(\mathbf{r}-\mathbf{z}_0)+\phi(\mathbf{r}+\mathbf{z}_0)]$, where $\phi(\mathbf{r})$ is the atomic wave function corresponding to the potential $U_0(\mathbf{r})$ and $C=\int\phi(\mathbf{r}-\mathbf{z}_0)\phi(\mathbf{r}+\mathbf{z}_0)d\mathbf{r}$ is the atomic orbital overlap integral [18]. The laser intensity is 4.7×10^{14} W/cm^2 and three frequencies are chosen. Figure 1 presents the angle-resolved HATI spectra with $\omega=0.057$ [(a) and (d)], 0.086 [(b) and (e)], and 0.114 [(c) and (f)] for the H_2^+ molecule [(a)–(c)] and the atomic xenon [(d)–(f)] for comparison. The ponderomotive energy U_p is 16.0ω, 4.7ω, and 2.0ω for $\omega=0.057$, 0.086, and 0.114, respectively. In Fig. 1, θ_f is the angle between the final momentum of the ionized electron and the molecular axis. The cutoff of the kinetic energy spectrum at $\theta_f=0$ is seen to be around $10U_p$ for all the three cases. Let us now compare the molecular case (left panels) with the atomic case (right panels) in Fig. 1. First, there are common interference fringes, which we define as the "background" interference due to $\Delta\Theta$ in both the molecular and atomic cases. These interference fringes reduce as the laser frequency increases. Second, there exist additional low-density areas in the molecular case [dashed curves in Figs.

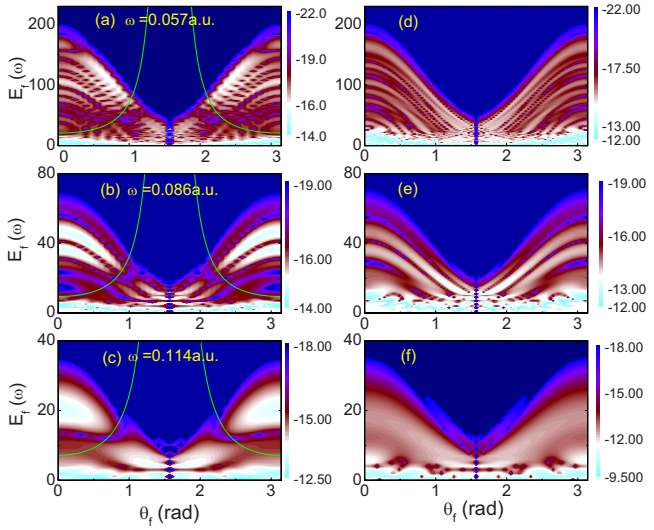

FIG. 1. (Color online) Angle-resolved HATI spectra with frequency $\omega=0.057$ [(a) and (d)], 0.086 [(b) and (e)], and 0.114 [(c) and (f)] for H_2^+ molecule [(a)-(c)] and Xe atom [(d)-(f)]. The meaning of the solid lines plotted here is the same as in Fig. 3. The results are plotted in log scale.

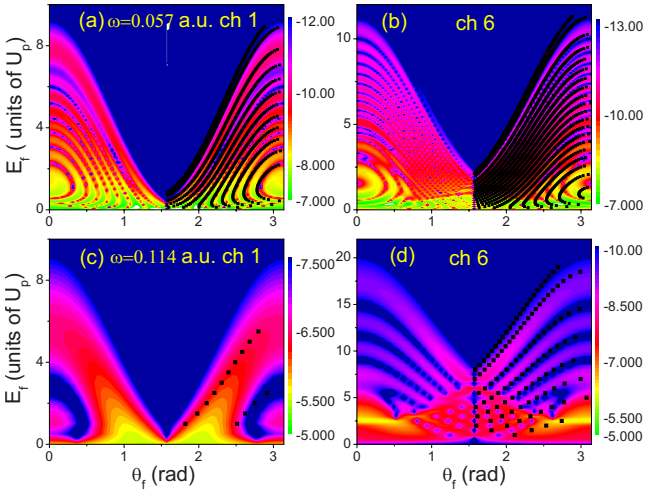

FIG. 2. (Color online) Angle-resolved HATI spectra of Xe with $\omega=0.057$ [(a) and (b)] and 0.114 [(c) and (d)] for channel 1 [(a) and (c)] and channel 6 [(b) and (d)]. The lines from by the squares are obtained by setting the cosine function cos F in Eq. (3) to be zero. The results are plotted in log scale.

1(a)–1(c) guiding these low-density areas will be discussed below], which is also mentioned in [4,7]. Third, the additional structure due to the destructive interference in the molecular case becomes clearer in the HATI spectrum as the laser frequency increases.

To gain more insights into the common features shared by atomic and molecular cases, we first analyze the LAC transition for separated ATI channels of the xenon atom and apply the saddle-point approximation to express Eq. (2) as follows:

$$T_{\mathrm{LAC}} = \frac{\omega}{\pi V_e}\langle \mathbf{p}_f|U|\mathbf{p}_1\rangle \sqrt{\frac{2\pi}{(\zeta_1-\zeta_f)\sin\,\omega t_1}}\cos F, \qquad (3)$$

where $\cos F \equiv \cos[s\omega t_1+(\zeta_1-\zeta_f)\sin\,\omega t_1-\pi/4]$ and t_1 is the saddle-point time satisfying $\cos(\omega t_1)=(p_f^2-p_1^2)/[4\sqrt{u_p\omega}\,(\mathbf{p}_1-\mathbf{p}_f)\cdot\hat{\boldsymbol{\epsilon}}]$, $s=(p_f^2-p_1^2)/(2\omega)$ is the number of photons absorbed during the collision. We find that the interference comes mainly from the cosine function cos F. The destructive interference lines should occur when $\cos F=0$. Figure 2 presents the angle-resolved HATI spectra of the xenon atom when $\omega=0.057$ [(a) and (b)] and $\omega=0.114$ [(c) and (d)] for channel 1 [(a) and (c)] and channel 6 [(b) and (d)], respectively (channel no. means the energy above the ionization threshold in terms of the number of photons). One finds that the number of interference fringes increases with channel order and decreases with frequency. The lines (connected by squares) in each panel of Fig. 2 are obtained by the formula $F=(2n+1)\pi/2$ with $n=0,\pm1,\pm2,\ldots$. For comparison, we only present the curves with $\theta_f\in(\pi/2,\pi)$ in Fig. 2. It is seen that the location of these lines agrees well with the actual minima from quantum calculations for all the cases shown in Fig. 2, except that the curves for the small E_f part in Fig. 2(b) are a little lower than the quantum results. This difference can be traced back to the error in the saddle-point approximation. As mentioned in [13], the phase factor in Eq. (2) can be regarded as due to the classical action difference of the classical trajectory before and after collision, i.e., $\Delta\Theta=\int_0^T dt\,\exp[-i\Delta S(t,\mathbf{p}_1,\mathbf{p}_f)]$ with $\Delta S(t,\mathbf{p}_1,\mathbf{p}_f)=S(t,\mathbf{p}_1)-S(t,\mathbf{p}_f)$, where the classical action is $S(t,\mathbf{p})=\frac{1}{2}\int dt\,[\mathbf{p}-\mathbf{A}_c(t)]^2$ with the potential of the corresponding classical laser field being $\mathbf{A}_c(t)=\sqrt{U_p}[\hat{\boldsymbol{\epsilon}}e^{-i\omega t}+\mathrm{c.c.}]$. Using the saddle-point approximation, we find that there are two moments t_1 and $2\pi/\omega-t_1$ that the rescattering occurs within one optical cycle, which corresponds to two classical trajectories; hence the interference fringes shown in Fig. 2 can be interpreted as the interference of these two classical trajectories, where the minima are determined by $F=(2n+1)\pi/2$. Although the function cos F is so complex that there is no direct way to show the relationship between the number of the interference fringes and the system condition, the results in Fig. 2 indicate that as U_p/ω or the incoming kinetic energy of the rescattering electron decreases, the number of interference fringes decreases as well. This is also clear from Eq. (2). For example, the variable of the Bessel function is scaled down as ω increases. Because the oscillation period of the Bessel function is fixed, increasing ω leads to larger period of oscillation in terms of $\mathbf{p}_1\cdot\hat{\boldsymbol{\epsilon}}$, and hence less interference fringes.

As an application, we now present the interference pattern of the HATI spectrum for different internuclear distances of H_2^+. Using the two-center potential of the molecule, the potential scattering matrix contained in T_{LAC} in Eq. (3) can be expressed as [4,7] $\langle \mathbf{p}_f|U|\mathbf{p}_1\rangle \propto \cos[\frac{R_0}{2}(p_f\cos\,\theta_f-p_1\cos\,\theta_1)]$, where θ_1 (θ_f) is the angle between the molecular axis and the momentum $\mathbf{p}_1$ ($\mathbf{p_f}$). Here because the main contribution comes from the first channel, we fixed $\mathbf{p}_1$ by the first channel, i.e., $|p_1|=\sqrt{2\omega\Delta E}$ with $\Delta E=\omega[\frac{E_B+U_p}{\omega}]+1-\frac{E_B+U_p}{\omega}$. Therefore, the condition $p_f\cos\,\theta_f-p_1\cos\,\theta_1=(2n+1)\pi/R_0$ yields the destructive minima in the interference fringes of the HATI spectrum. It is this mechanism that can be used to capture the characteristic of the geometrical structure of the

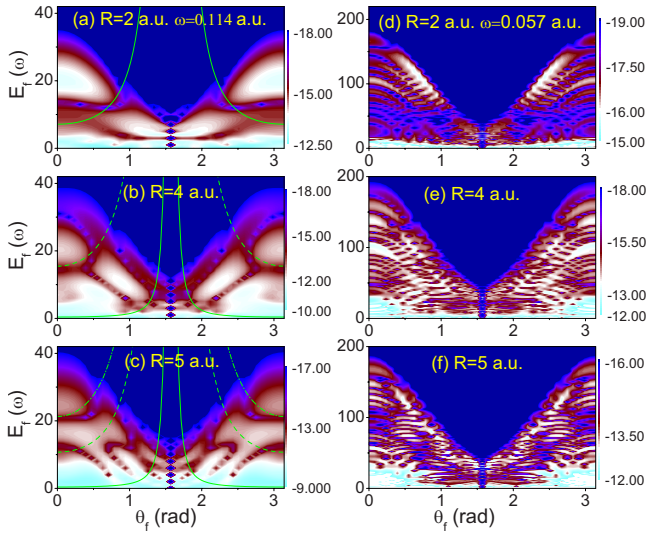

FIG. 3. (Color online) Angle-resolved HATI spectra of H_2^+ with the ω=0.114 ([(a)–(c)] and 0.057 [(d)–(f)] for the internuclear distance R_0=2.0 [(a) and (d)], 4.0 [(b) and (e)], and 5.0 [(c) and (f)]. The results are plotted in log scale.

molecule [4,7]. Figure 3 presents the HATI spectra of H_2^+ with R_0=2.0 (a), 4.0 (b), and 5.0 (c), for ω=0.114. For comparison, the parallel spectra with ω=0.057 are also presented in Figs. 3(d)–3(f). One finds that the molecular structure can be clearly imaged by the HATI spectrum in the left panels with the higher frequency. Furthermore, the locations of the spectrum minima can be well predicted by the formula $p_f \cos\theta_f + p_1 = \frac{(2n+1)\pi}{R_0}$ (n=1 for solid curve and n=2 for dashed curve) and $p_f \cos\theta_f - p_1 = \frac{(2n+1)\pi}{R_0}$ (n=1 for dash-dotted curve). The little discrepancy between the curves and the destructive minimum areas shown in Figs. 1(a)–1(c) and Figs. 3(a)–3(c) are caused by the other channel contributions where the corresponding $|p_1|$ has different values for different channels. Furthermore, we have checked that the "blurring effect" of the focal averaging of the laser intensity on the HATI spectrum is insignificant.

To conclude, the angle-resolved HATI spectrum of a molecule has been investigated by a time-independent scattering theory. All main interference features in the HATI spectrum have been explained, in terms of the molecular wave function in the direct ATI amplitude, the geometrical structure of the molecule, and the interaction between the ionized electron and the laser field. We have also proposed to use a laser with higher frequency for better molecular structure imaging.

This work was supported by NNSF of China (Grants No. 60478031 and No. 60708003), and the 973 project of China Grant No. 2006CB806003. Z.C.Y was supported by NSERC of Canada. J.G. was supported by the NUS "YIA" (WBS Grant No. R-144-000-195-101). B.W. thanks Biao Wu and Jing Chen for helpful suggestions.

[1] J. Itatani *et al.*, Nature (London) **432**, 867 (2004); S. Baker *et al.*, Science **312**, 424 (2006); X. Zhou, R. Lock, W. Li, N. Wagner, M. M. Murnane, and H. C. Kapteyn, Phys. Rev. Lett. **100**, 073902 (2008); B. K. McFarland *et al.*, Science **322**, 1232 (2008); W. Li *et al.*, *ibid.* **322**, 1207 (2008).
[2] S. Odžak and D. B. Milosevic, J. Phys. B **42**, 071001 (2009).
[3] M. Lein, N. Hay, R. Velotta, J. P. Marangos, and P. L. Knight, Phys. Rev. Lett. **88**, 183903 (2002); T. Morishita, A. T. Le, Z. Chen, and C. D. Lin, *ibid.* **100**, 013903 (2008).
[4] H. Hetzheim, C. Figueira de Morisson Faria, and W. Becker, Phys. Rev. A **76**, 023418 (2007).
[5] M. Lein, J. P. Marangos, and P. L. Knight, Phys. Rev. A **66**, 051404 (2002); H. Niikura *et al.*, Nature (London) **417**, 917 (2002); M. Lein, J. Phys. B **40**, R135 (2007).
[6] M. Meckel *et al.*, Science **320**, 1478 (2008).
[7] M. Busuladžić, A. Gazibegović-Busuladžić, D. B. Milošević, and W. Becker, Phys. Rev. Lett. **100**, 203003 (2008); Phys. Rev. A **78**, 033412 (2008).
[8] M. Okunishi, R. Itaya, K. Shimada, G. Prumper, K. Ueda, M. Busuladzic, A. Gazibegovic-Busuladzic, D. B. Milosevic, and W. Becker, Phys. Rev. Lett. **103**, 043001 (2009).
[9] H. R. Reiss, Phys. Rev. Lett. **102**, 143003 (2009).
[10] D.-S. Guo, T. Aberg, and B. Crasemann, Phys. Rev. A **40**, 4997 (1989).
[11] L. Gao, X. Li, P. Fu, R. R. Freeman, and D. S. Guo, Phys. Rev. A **61**, 063407 (2000).
[12] P. Fu, B. Wang, X. Li, and L. Gao, Phys. Rev. A **64**, 063401 (2001); T. Cheng, X. Li, S. Ao, L. A. Wu, and P. Fu, *ibid.* **68**, 033411 (2003).
[13] B. Wang, L. Gao, X. Li, D. S. Guo, and P. Fu, Phys. Rev. A **75**, 063419 (2007).
[14] M. Gell-Mann and M. L. Goldberger, Phys. Rev. **91**, 398 (1953); M. L. Goldberger and K. M. Watson, *Collision Theory* (Wiley, New York, 1964).
[15] M. Jain and N. Tzoar, Phys. Rev. A **18**, 538 (1978).
[16] H. R. Reiss, Phys. Rev. A **22**, 1786 (1980).
[17] X. Y. Jia, W. D. Li, J. Fan, J. Liu, and J. Chen, Phys. Rev. A **77**, 063407 (2008).
[18] V. I. Usachenko and Shih-I Chu, Phys. Rev. A **71**, 063410 (2005).